IOP Publishing Journal of Micromechanics and Microengineering

J. Micromech. Microeng. **26** (2016) 045001 (9pp) doi:10.1088/0960-1317/26/4/045001

Study on a flexoelectric microphone using barium strontium titanate

S R Kwon[1], W B Huang[2], S J Zhang[3], F G Yuan[2] and X N Jiang[2]

[1] Institute of Mechanical Engineering Technology, Kyungpook National University, Daegu, Korea
[2] Department of Mechanical and Aerospace Engineering, North Carolina State University, Raleigh, NC 27695, USA
[3] Materials Research Institute, Pennsylvania State University, University Park, PA 16802, USA

E-mail: seolr.kwon@gmail.com

Received 18 June 2015, revised 28 December 2015
Accepted for publication 11 January 2016
Published 22 February 2016

Abstract

In this study, a flexoelectric microphone was, for the first time, designed and fabricated in a bridge structure using barium strontium titanate ($Ba_{0.65}Sr_{0.35}TiO_3$) ceramic and tested afterwards. The prototyped flexoelectric microphone consists of a 1.5 mm $\times$ 768 μm $\times$ 50 μm BST bridge structure and a silicon substrate with a cavity. The sensitivity and resonance frequency were designed to be 0.92 pC/Pa and 98.67 kHz, respectively. The signal to noise ratio was measured to be 74 dB. The results demonstrate that the flexoelectric microphone possesses high sensitivity and a wide working frequency range simultaneously, suggesting that flexoelectricity could be an excellent alternative sensing mechanism for microphone applications.

Keywords: flexoelectricity, microphone, barium strontium titanate, micro-bridge

(Some figures may appear in colour only in the online journal)

1. Introduction

The microphones used in mobile phones, computers, and artificial hearing aids require high performance and low cost. This is especially true for hearing aids, where microphones must be compact and highly sensitive with a wide bandwidth to cover the entire frequency range of audible sound.

Generally, capacitive, fiber optic, piezoresistive and piezoelectric microphones have been used for acoustic sensing. However, each of these acoustic sensor types has advantages and disadvantages. For example, although capacitive microphones have been commercialized due to their high sensitivity, high signal to noise ratio and high stability [1–3], they nevertheless suffer from a complex structure and fabrication process. In addition, they need an external DC voltage supply to detect capacitance changes. Therefore, the high standby power consumption leads to the inconvenience of frequent battery replacements [4]. Fiber optic microphones [5, 6] have been used in harsh environments because they are not influenced by electrical, magnetic or radioactive fields. However, they have relatively low sensitivity and durability, and are also costly and difficult to repair [7, 8]. Piezoresistive and piezoelectric microphones [4, 9] have frequently been used for acoustic sensing because they are desirable due to their simple and robust mechanical structures. However, they are known to have low sensitivity and narrow bandwidth. The reason for this is that the resonance and sensitivity of microphones are solely dependent on the dimensions and material properties, therefore there is a trade-off relationship between them. They also have a limited operating temperature range because above a certain temperature point, known as the Curie temperature, the piezoelectricity starts to disappear. Moreover, the most sensitive piezoelectric microphones are usually composed of lead based ceramics, leading to health concerns for humans [10].

In this research, a new type of microphone using the flexoelectric material, barium strontium titanate ($Ba_{0.65}Sr_{0.35}TiO_3$ or BST), was proposed to enhance the sensor sensitivity and bandwidth. Flexoelectricity has several advantages as a sensing principle. In crystallography, flexoelectricity can be found in all dielectric solids. On the other hand, piezoelectricity exists in only non-centrosymmetric crystal systems, a total of 20 out of 32 point groups [11, 12]. This indicates that flexoelectricity offers a broader choice of

materials for electromechanical sensing with preferable properties. Of particular significance is the fact that flexoelectricity is not based on remnant polarization, and hence the poling process is not required for utilization. This being so, flexoelectric materials do not exhibit poling related aging problems [13, 14]. Furthermore, thanks to the scaling effect, flexoelectric sensing structures are expected to exhibit much higher sensitivity when the structures are scaled down to micro/nano domains [15–17].

The sensing material BST was chosen because it has the highest reported flexoelectric properties [18] ($\mu_{12} \sim 100\,\mu\mathrm{C\,m^{-1}}$ at Curie temperature) among reported ceramics in literatures [12, 19–22]. Also, BST has been demonstrated in several types of sensors such as accelerometer [15] and curvature sensors [23]. In this paper, a bridge-structured flexoelectric microphone using BST is, for the first time, designed, fabricated and tested. Theoretical analysis is also carried out for flexoelectric sound sensing and compared with experimental measurements.

2. Experimental design

Flexoelectricity is defined as the linear energy coupling between the strain gradient and the induced electric polarization [24–26]. This is characterized by a tensorial relationship;

$$P_l = \mu_{ijkl}\frac{\partial \varepsilon_{ij}}{\partial x_k} \tag{1}$$

where P_l is the component of flexoelectric polarization; μ_{ijkl} is the flexoelectric coefficients, a fourth rank tensor; ε_{ij} is the mechanical strain tensor; and x_k is the direction of the gradient in ε_{ij}.

For a cubic crystal such as BST, the non-zero components of μ_{ijkl} are μ_{1111}, μ_{1122}, and μ_{1212} or, in matrix notation, μ_{11}, μ_{12} and μ_{44}. Each flexoelectric coefficient is associated with a specific mode; μ_{11} with axial, μ_{12} with bending, and μ_{44} with shear modes.

2.1. Sensing structure

Three different modes of flexoelectricity including compression, shear and bending modes can be adopted in sensor designs. The corresponding flexoelectric coefficients are μ_{11}, μ_{44} and μ_{12}, respectively. In order to generate a large strain gradient, the bending or flexural mode was considered in this design. Figure 1 shows the schematic views of three main flexural mode sensing structures, namely the membrane, bridge and cantilever structure, which are also the main structures for piezoelectric microphones. Due to the symmetry of the structures, the strain gradient distribution has different signs at different locations, which can lead to cancellation of the electric charge output if a fully covered electrode pattern is used. To avoid this problem and to maximize the sensitivity, the electrode layout should be optimized to collect the single signed flexoelectric polarization, either the positive or negative.

From the Euler–Bernoulli beam theory, the deflection of the three flexural structures due to an external pressure can be estimated as

$$\begin{cases} \delta_M(r) = \dfrac{Pa^4}{64D}\left(1-\dfrac{r^2}{a^2}\right)^2 \quad \text{where } D = \dfrac{Et^3}{12(1-\nu^2)} \\ \delta_B(x) = \dfrac{PL^2x^2}{24EI}\left(1-\dfrac{x}{L}\right)^2 \\ \delta_C(x) = \dfrac{Px^2}{24EI}(6L^2-4Lx+x^2) \end{cases} \tag{2}$$

where δ, P, t, a, L, ν and EI represent the deflection, external pressure, thickness, radius of membrane, length of bridge, Poisson's ratio and bending rigidity of inertia of bridge and cantilever, respectively. Here, the super/subscript M, B and C denote the membrane, bridge and cantilever structures, respectively. The values r and x are the arbitrary coordinates from the center of the circular membrane or the cantilever to their clamped sides.

The flexoelectric polarization of the bridge (P_3^{B}) and cantilever structures (P_3^{C}) due to the gradient of strain can be simplified as [25]

$$\begin{aligned} P_3^{\mathrm{B,C}} &= \mu_{11}\frac{\partial \varepsilon_{33}}{\partial z} + \mu_{12}\left(\frac{\partial \varepsilon_{11}}{\partial z}+\frac{\partial \varepsilon_{22}}{\partial z}\right) = [\nu\mu_{11}+(1+\nu)\mu_{12}]\frac{\partial \varepsilon_{11}}{\partial z} \\ &= \mu_{12}^{\mathrm{eff}}\frac{\partial \varepsilon_{11}}{\partial z} = \mu_{12}^{\mathrm{eff}}\frac{\partial}{\partial z}\left(\frac{z}{R}\right) = \mu_{12}^{\mathrm{eff}}\frac{1}{R} = \mu_{12}^{\mathrm{eff}}\frac{\partial^2 \delta_{\mathrm{B,C}}(x)}{\partial x^2} \end{aligned} \tag{3}$$

where R is the radius of the curvature. Similarly, the flexoelectric polarization of the circular membrane (P_3^{M}) can be simplified as

$$P_3^{\mathrm{M}} = \mu_{12}^{\mathrm{eff}}\frac{\partial^2 \delta_{\mathrm{M}}(r)}{\partial r^2} \tag{4}$$

The charge outputs ($Q_{\mathrm{M,B\ and\ C}}$) induced by external pressure (P) of each structure can be calculated and simplified by the integration of the polarization.

$$\begin{cases} Q_{\mathrm{M}} = \displaystyle\int_0^{2\pi}\int_b^a P_3^{\mathrm{M}}\mathrm{d}r\mathrm{d}\theta = \mu_{12}^{\mathrm{eff}}\frac{P\pi b}{8D}(a^2-b^2) \\ Q_{\mathrm{B}} = \displaystyle\int_0^{w}\int_0^{l_{\mathrm{B}}} P_3^{\mathrm{B}}\mathrm{d}x\mathrm{d}y = \mu_{12}^{\mathrm{eff}}\frac{Pwl_{\mathrm{B}}(2l_{\mathrm{B}}^2-3l_{\mathrm{B}}L+L^2)}{12EI} \\ Q_{\mathrm{C}} = \displaystyle\int_0^{w}\int_0^{l_{\mathrm{C}}} P_3^{\mathrm{C}}\mathrm{d}x\mathrm{d}y = \mu_{12}^{\mathrm{eff}}\frac{Pwl_{\mathrm{C}}(l_{\mathrm{C}}^2-3l_{\mathrm{C}}L+3L^2)}{6EI} \end{cases} \tag{5}$$

where b, l_{B} and l_{C} are the inner radius of electrode of the circular membrane, electrode lengths of the bridge and cantilever from the clamped sides, respectively.

The electrode sizes that maximize the charge output of each structure can be determined as follows.

$$\begin{cases} b = \dfrac{a}{\sqrt{3}} \\ l_{\mathrm{B}} = \dfrac{3-\sqrt{3}}{6}L \\ l_{\mathrm{C}} = L \end{cases} \tag{6}$$

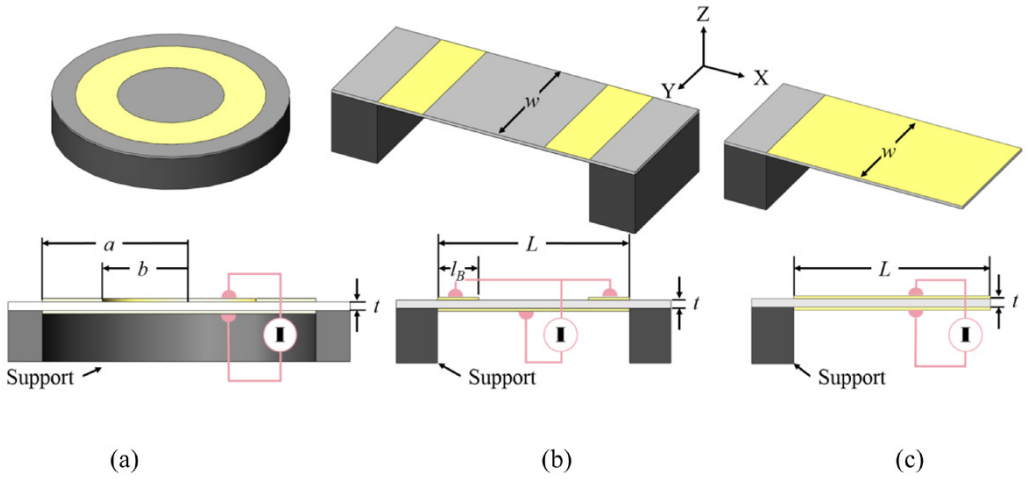

Figure 1. Basic structures for microphones using bending mode and their cross section views. (a) Circular membrane, (b) bridge, and (c) cantilever (grey area: flexoelectric material, yellow area: electrode, dark gray area: silicon substrate-support, and pink line: electric connection).

Table 1. Summary of electrode area, sensitivity and resonance for various microphone structures [28].

	Membrane	Bridge	Cantilever
Electrode area[a]	$\frac{2}{3}\pi r^2 = 1.58A_B$	$2\times\frac{3-\sqrt{3}}{6}L\times w = A_B$	$L\times w \approx 2.37A_B$
Sensitivity	$\mu_{12}\frac{a^3\pi(1-\nu^2)}{\sqrt{3}Et^3}\approx 0.56S_B$	$\mu_{12}\frac{wL^3}{36\sqrt{3}EI} = S_B$	$\mu_{12}\frac{wL^3}{6EI}\approx 10.39S_B$
Resonance	$\frac{2.94}{2\pi}\sqrt{\frac{Et^2}{\rho a^4(1-\nu^2)}}\approx 2.93f_B$	$\frac{4.73^2}{2\pi}\sqrt{\frac{EI}{\rho wtL^4}} = f_B$	$\frac{1.8751^2}{2\pi}\sqrt{\frac{EI}{\rho wtL^4}}\approx 0.16f_B$

[a] The active area and thickness of three structures are the same and $\nu = 0.3$ for BST.

The non-resonance typed sensors like these flexoelectric microphones only utilize a low frequency range. The operating frequency range is defined as a low frequency range which is flat. Typically, the operating frequency range of this type of sensor is from three over the time constant (τ) to one fourth of the resonance frequency. The low frequency response is limited by the time constant while the high frequency range is limited by mechanical resonance (ω_n) [27]. And the sensitivity at low frequency can be simply calculated by dividing the charge output by an external pressure.

The optimized electrode size, sensitivity and resonance for three different structures are summarized and listed in table 1. In order to compare the sensitivities and resonances of these three structures, the values of the bridge shape structure were used as a reference. It can be observed that the cantilever-structured microphone can generate the highest sensitivity, which is more than 10 times larger than the bridge structure. The high flexibility of the cantilever structure lowers the resonance frequency by a factor of 0.16 than the bridge microphones. The bridge structure was then chosen due to its wide bandwidth and moderate sensitivity. The following section will focus on the modeling of the bending type bridge-structured flexoelectric microphone.

2.2. Flexoelectric microphone design

The configuration and side view of the flexoelectric microphone are shown in figure 2. The resonance frequency of the flexoelectric microphone structure was first calculated since the resonance is usually associated with the bandwidth of a sensor. Considering a beam with two fixed ends, the first natural frequency can be calculated as

$$f_0 = \frac{4.73^2}{2\pi}\sqrt{\frac{EI}{\rho AL^4}} \tag{7}$$

where EI, ρ, A and L are the bending rigidity, density, cross section area and length of the BST bridge, respectively.

As mentioned earlier, the charge output becomes the maximum when $l_B = (3-\sqrt{3})L/6$ and the two electrodes are connected in parallel in order to amplify the charge output. Then the final charge output can be derived as

$$Q = \mu_{12}^{\text{eff}}\frac{L^3 w}{36\sqrt{3}EI}P. \tag{8}$$

The sensitivity of the flexoelectric microphone is calculated by dividing the charge output (Q) by the external pressure (P):

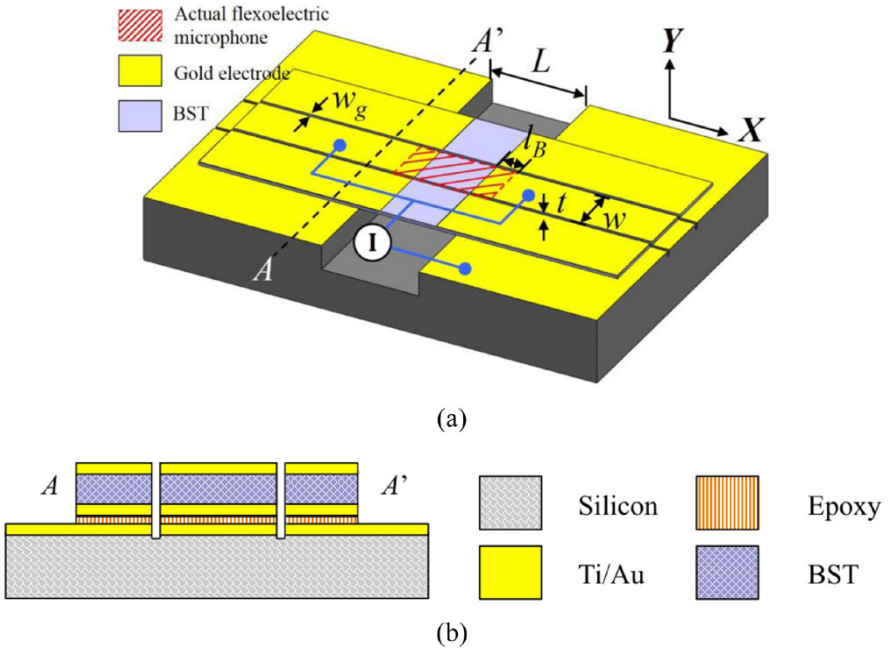

Figure 2. Schematic view of a flexoelectric microphone. (a) Configuration of the microphone and (b) side-view of the microphone across A and A′.

Table 2. Dimensions of the microphone structure and material properties of BST.

L (mm)	l_B (μm)	t (μm)	w (μm)	w_g (μm)	μ_{12} (μC m^{-1})	ρ (kg m^{-3})	E (GPa)	ε_r
1.5	317	50	768	50	30	8200	153	8000

$$S = \mu_{12}^{\text{eff}} \frac{L^3 w}{36\sqrt{3}EI}. \tag{9}$$

Based on the calculation with the given dimensions in table 2, the resonance and sensitivity of the device become 93.73 kHz and 0.92 pC Pa^{-1}, respectively.

The frequency response can be analytically predicted by a second-order system with a transfer function given by

$$H(s) = \frac{A}{s^2 + Bs + C}. \tag{10}$$

Constants A, B and C are related to the microphone's frequency response through $A = C\ S_{\text{low}}$, $B = 2\pi f_0/Q_m$ and $C = (2\pi f_0)^2$, where S_{low} is the low-frequency sensitivity and Q_m is the quality factor. Q_m will be calculated from experimental measurements:

$$Q_m = \frac{f_0}{f_2 - f_1} \tag{11}$$

where f_1 and f_2 are two measured frequencies where the signal becomes 3 dB lower than that at resonance f_0.

2.3. Fabrication

To fabricate a flexoelectric microphone, Ti/Au electrodes on the top side of a silicon wafer and bottom side of a BST ceramic plate were deposited by e-beam sputtering with the thickness of 10 nm and 100 nm, respectively. A 1.5 mm wide trench was made by dicing (DAD321, Disco Corp., Tokyo, Japan), as shown in figure 3(a), and then the BST ceramic was bonded onto the Si substrate with epoxy (EP301, Epoxy Technology, Billerica, MA) under the normal pressure of 1 MPa (figure 3(b)). The bottom of the ceramic was filled with wax (0CON-193, Logitech Limited, Glasgow, UK) to protect the BST ceramic during the followed lapping and dicing steps (figure 3(c)). The BST layer was lapped down to 50 μm thick and the Ti/Au top electrode was deposited by the e-beam evaporation and patterned with a lift-off process (figure 3(d)). The layer was next diced into the final dimensions (figure 3(e)) as shown in table 2 with a 50 μm thick dicing blade. The wax was removed using the Ecoclear solution (0CON-178, Logitech Limited, Glasgow, UK) (figure 3(f)). Finally, wires to collect the charge were bonded to the two top electrodes and bottom electrode with silver epoxy (8331, MG Chemical, Ontario, Canada). The two top wires were connected together forming a terminal for charge measurement with the wire of the bottom electrode. Figure 4 shows the photograph of the fabricated flexoelectric microphone.

The $Ba_{0.65}Sr_{0.35}TiO_3$ has a Curie temperature of 20 °C [29] and the experiments were carried out at room temperature of 23 °C.

2.4. Experimental setup

The flexoelectric microphone, a reference microphone and a loud speaker were placed in an anechoic box at room

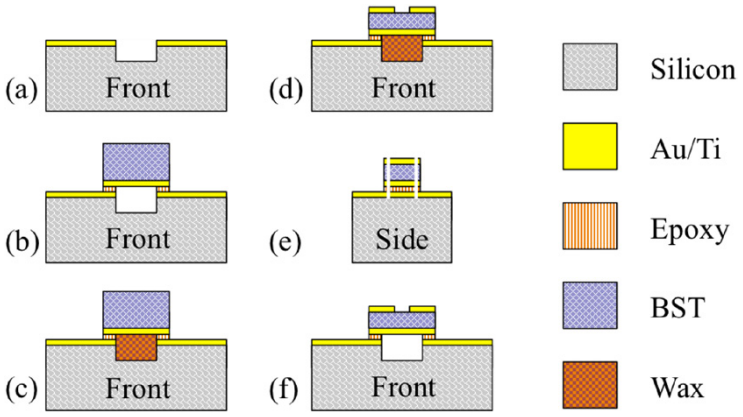

Figure 3. Fabrication process of the flexoelectric microphone.

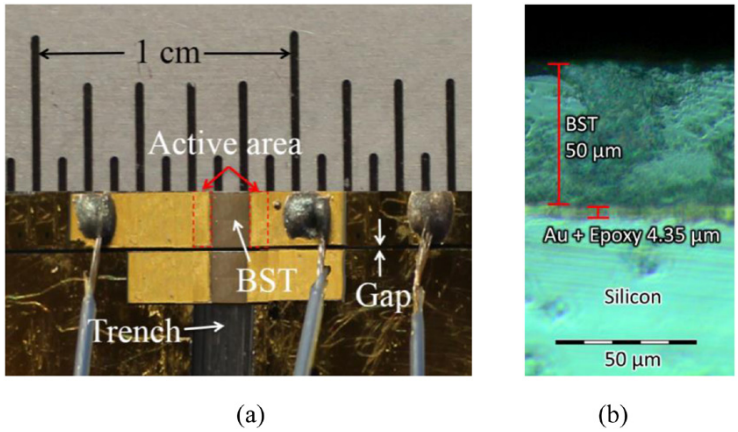

Figure 4. Photograph of the flexoelectric microphone. (a) Top view and (b) side view.

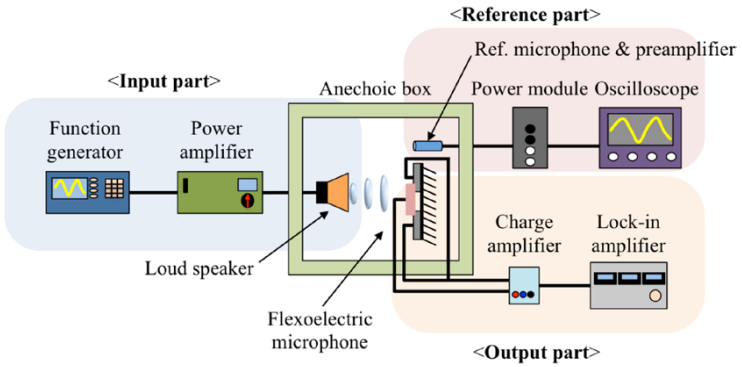

Figure 5. Experimental set-up for flexoelectric microphone tests.

temperature in order to reduce reflective sound pressure. The experimental setup is schematically shown in figure 5. The flexoelectric microphone and a loud speaker (KPSG-100, Kingstate Electronics Corp., New Taipei City, Taiwan) were facing to each other. The loud speaker was driven by a power amplifier (Type 2706, Brüel & Kjær, Nærum, Denmark) and a function generator (AFG3101, Tectronix Inc., Beaverton, OR). Then, the flexoelectric microphone and a reference microphone (46BG & 46DP, G.R.A.S. Sound & Vibration, Holte, Denmark) were used to measure the acoustic pressure generated by the loud speaker. Here, the reference microphone was powered by a power module (G.R.A.S. 12AK). The reference pressure was obtained by processing the signal from the power module with an oscilloscope (DSO7104B, Agilent Technologies Inc., Santa Clara, CA). The generated output signal from the flexoelectric microphone was amplified by a charge amplifier (Type 2635, Brüel & Kjær, Nærum, Denmark) and the amplified signal was digitized by a lock-in amplifier (SR830, Stanford Research system, Sunnyvale, CA).

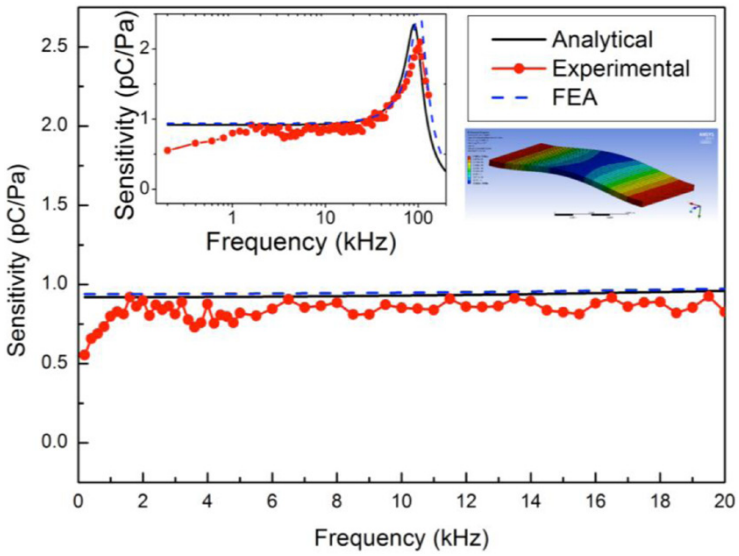

Figure 6. The analytical, experimental and FEA sensitivity of the flexoelectric microphone at low frequency range (inset: overall sensitivity).

3. Results

The output charge from the flexoelectric microphone was measured by a lock-in-amplifier. The resulting sensitivity was then calculated by dividing the output charge by the pressure measured by the reference microphone. The test frequency range was from 0.1 to 130 kHz as shown in figure 6. Experimental result was compared with analytical and FEA results which were obtained from equation (10) and Ansys, respectively. The expected response of the microphone was calculated by making analytical Bode plot with the measured value of Q_m, expected resonance frequency and low frequency sensitivity. For the FEA solution, the bridge was meshed with hexahedral elements in fine-level size. The total number of elements was 5856. The beam was fixed at the both ends and the sinusoidal pressure with amplitude of 1 Pa was applied on the one top surface. The frequency of the applied pressure was swept from 0 to 100 kHz.

As shown in the inset of figure 6, the sensitivity at working frequency range (1–20 kHz), which can be defined by flat response range at low frequency, was measured to be 0.85 pC Pa^{-1}. From 20 kHz, the sensitivity starts to increase and becomes maximum at 104 kHz.

The experimental results agree well with the analytical solution and FEA result. Table 3 summarizes the measured parameters. Figure 7 shows the sensor output as a function of pressure under different frequencies. Linearity between the pressure and charge output at 0.5, 1, 5, 10, 15 and 20 kHz can be observed, indicating a broad bandwidth of the sensor. Each measurement set at different frequencies is linear ($R^2 = 0.9997$) and has sensitivity of 0.77–0.85 pC Pa^{-1}. The average is 0.81 pC Pa^{-1} and standard deviation is approximately 0.03 pC Pa^{-1}. Once can see that the measured sensitivity is close to the analytical value.

Table 3. Comparison of analytical, FEA and experimental results of resonance frequency (f_0) and sensitivities.

	Analytical	FEA	Experimental
f_0 (kHz)	93.73	102	104
Sensitivity at 10 kHz (pC Pa^{-1})	0.93	0.95	0.86
Sensitivity at f_0 (pC Pa^{-1})	2.32	2.55	2.25

In addition to the sensitivity, the signal-to-noise ratio at frequencies ranging from 1 to 20 kHz was measured using the similar setup. The function generator and the power amplifier were maintained while disconnected with the loud speaker, thus remaining the electromagnetic noise. The output charges were measured from the lock-in amplifier as the noise signal. Figure 8 shows the signal-to-noise ratio of the flexoelectric microphone at 1 Pa. The charge output at 1 Pa is 5000 times larger than that of surrounding noise sources induced by the measurement equipment, corresponding to 74 dB.

4. Discussion

Small discrepancies were found in the frequency response of the experiment and analytical solution. Mostly arise from fabrication related imperfections. For example, a small amount of residual wax that was used to protect the BST bridge during dicing can act as additional mass, thus increasing the resonance frequency and making the sensitivity lower than expected. In addition, if the top two electrodes are not placed as designed, the collected charge may not be the maximum as designed and lead to reduced sensitivity. Much lower sensitivity, which is called roll-off sensitivity, can be observed below 1 kHz. This is most likely caused by the equalization of the pressure difference associated with acoustic wave [4].

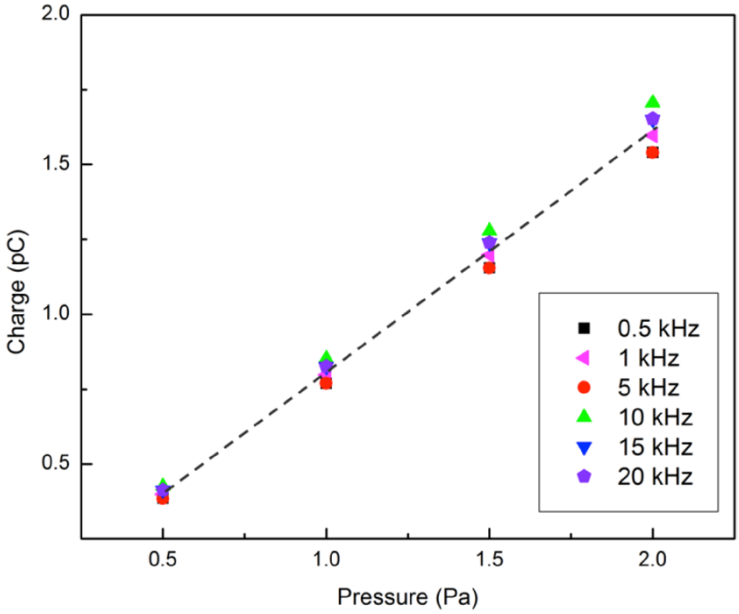

Figure 7. Sensor charge outputs under different frequencies and pressure values.

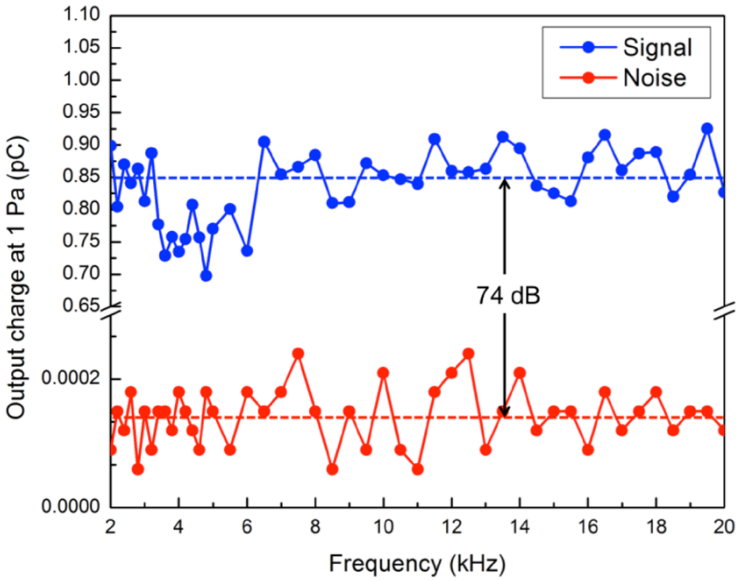

Figure 8. The signal to noise ratio of the flexoelectric microphone at 1 Pa.

Moreover, the flexoelectric microphone reported in this paper exhibits promising results including both high sensitivity and wide bandwidth. The results were compared to various types of microphones [4, 9, 30–34], as shown in tables 4 and 5.

The charge sensitivity obtained above was converted to the voltage sensitivity for comparison as follows:

$$S_v = \frac{S_c}{C}. \tag{12}$$

Table 4. General performance information of the flexoelectric microphone and other microphones [7, 8, 35, 36].

	Capacitive	Optical	Piezoelectric	Flexoelectric (Current study)
Sensitivity	0.4–50 (mV Pa^{-1})	1–100 (μV Pa^{-1})	10–500 (μV Pa^{-1})	0.63 (mV Pa^{-1})
Input power	Required	Required	None	None
Dynamic range	Narrow	Relatively wide	Wide	Wide

Table 5. Performance of the flexoelectric microphone compared to notable microphones from the literatures and commercial.

Author	Material	Structure	Area × thickness ($mm^2 \times \mu m$)	Sensitivity ($mV\ Pa^{-1}$)	Resonance or bandwidth (kHz)
Capacitive microphone					
Martin [37]	Polysilicon	Membrane	0.166 × 2.25	390	0.03–20 Bandwidth
Scheeper [38]	Si_3N_4	Membrane	2.99 × 0.5	22.4	0.251–20 Bandwidth
Optical microphone					
MO 2000H optical microphone (Sennheiser)	N/A	Membrane	External diameter 1/2″	15	0.02–40 Bandwidth
Piezoelectric microphone					
Baumgartel [39]	ZnO	Cantilever	0.83 × 4.5	0.17	5.997 Resonance
Prasad [1]	ZnO	Membrane	9.61 × 30	0.335	4.0 Resonance
Flexoelectric microphone					
Current study	BST	Bridge	1.152 × 50	0.63	93.7 Resonance

Here, S_c S_v and C are the charge sensitivity, voltage sensitivity of the flexoelectric microphone and measured capacitance of BST.

5. Conclusions

In summary, by using a barium strontium titanate ($Ba_{0.67}Sr_{0.33}TiO_3$) ceramic which exhibits μ_{12} of 30 $\mu C\ m^{-1}$, a flexoelectric microphone was designed, fabricated and tested. The designed sensitivity of the fabricated microphone was 0.92 pC Pa^{-1} in the audible range of 1–20 kHz. The experimental results showed a sensitivity of 0.85 pC Pa^{-1} with the signal-to-noise ratio of 74 dB. The flexoelectric microphone presented in this paper offers both high sensitivity and wide bandwidth compared to existing piezoelectric microphones. Therefore, the flexoelectric effect could be an effective and promising alternative sensing mechanism for better performance in many areas.

Acknowledgments

This material is based upon work supported by, or in part by, the US Army Research Laboratory and the US Army Research Office under contract/grant number W911NF-11-1-0516; and in part by National Science Foundation under grant number CMMI-1068345.

References

[1] Prasad M, Yadav R, Sahula V and Khanna V 2012 Design and mathematical model of a ZnO-based MEMS acoustic sensor *16th Int. Workshop on Physics of Semiconductor Devices* (Bellingham, WA: International Society for Optics and Photonics) p 85491D-D-9

[2] Weigold J, Brosnihan T, Bergeron J and Zhang X 2006 A MEMS condenser microphone for consumer applications *19th IEEE Int. Conf. on Micro Electro Mechanical Systems (Istanbul)* (Piscataway, NJ: IEEE) pp 86–9

[3] Ganji B A and Majlis B Y 2009 Design and fabrication of a new MEMS capacitive microphone using a perforated aluminum diaphragm *Sensors Actuators* A **149** 29–37

[4] Rogalski A 2011 Recent progress in infrared detector technologies *Infrared Phys. Technol.* **54** 136–54

[5] Cao H, Schmidt V H, Zhang R, Cao W and Luo H 2004 Elastic, piezoelectric, and dielectric properties of 0.58Pb ($Mg_{1/3}$ $Nb_{2/3}$) $O_{3-0.42}PbTiO_3$ single crystal *J. Appl. Phys.* **96** 549–54

[6] Chen L, Chan C, Yuan W, Goh S and Sun J 2010 High performance chitosan diaphragm-based fiber-optic acoustic sensor *Sensors Actuators* A **163** 42–7

[7] Eargle J 2012 *The Microphone Book: from Mono to Stereo to Surround—A Guide to Microphone Design and Application* (Boca Raton, FL: CRC)

[8] Kwon S R, Huang W, Zhang S, Yuan F-G and Jiang X 2014 A new type of microphone using flexoelectric barium strontium titnate *SPIE Smart Structures and Materials + Nondestructive Evaluation and Health Monitoring* (Bellingham, WA: International Society for Optics and Photonics) p 90620Y-Y-7

[9] Tahan D M, Safari A and Klein L C 1996 Preparation and characterization of Ba_xSr_{1-x}, TiO_3 thin films by a sol-gel technique *J. Am. Ceram. Soc.* **79** 1593–8

[10] Hartzell J W, Zhan C and Wolfson M B 2008 MEMS pixel sensor *Google Patents, USA*

[11] Huang W, Kim K, Zhang S, Yuan F-G and Jiang X 2011 Scaling effect of flexoelectric (Ba,Sr)TiO_3 microcantilevers *Phys. Status Solidi* **5** 350–2

[12] Zhu W, Fu J Y, Li N and Cross L 2006 Piezoelectric composite based on the enhanced flexoelectric effects *Appl. Phys. Lett.* **89** 192904–3

[13] Pulskamp J S, Wickenden A, Polcawich R, Piekarski B, Dubey M and Smith G 2003 Mitigation of residual film stress deformation in multilayer microelectromechanical systems cantilever devices *J. Vac. Sci. Technol.* B **21** 2482–6

[14] Lee D, Yoon A, Jang S, Yoon J G, Chung J S, Kim M, Scott J and Noh T 2011 Giant flexoelectric effect in ferroelectric epitaxial thin films *Phys. Rev. Lett.* **107** 57602

[15] Chu B, Zhu W, Li N and Cross L E 2009 Flexure mode flexoelectric piezoelectric composites *J. Appl. Phys.* **106** 104109–3

[16] Kwon S, Huang W, Zhang S, Yuan F and Jiang X 2013 Flexoelectric sensing using a multilayered barium strontium titanate structure *Smart Mater. Struct.* **22** 115017

[17] Horikawa T, Mikami N, Makita T, Tanimura J, Kataoka M, Sato K and Nunoshita M 1993 Dielectric properties of (Ba, Sr) TiO_3 thin films deposited by RF sputtering *Japan. J. Appl. Phys* **32** 4126

[18] Ma W and Cross L E 2002 Flexoelectric polarization of barium strontium titanate in the paraelectric state *Appl. Phys. Lett.* **81** 3440–2
[19] Ma W and Cross L E 2005 Flexoelectric effect in ceramic lead zirconate titanate *Appl. Phys. Lett.* **86** 072905–3
[20] Ma W and Cross L E 2006 Flexoelectricity of barium titanate *Appl. Phys. Lett.* **88** 232902–3
[21] Ma W and Cross L E 2001 Observation of the flexoelectric effect in relaxor $Pb(Mg_{1/3}Nb_{2/3})O_3$ ceramics *Appl. Phys. Lett.* **78** 2920–1
[22] Zubko P, Catalan G, Buckley A, Welche P and Scott J 2007 Strain-gradient-induced polarization in $SrTiO_3$ single crystals *Phys. Rev. Lett.* **99** 167601
[23] Huang W, Yan X, Kwon S R, Zhang S, Yuan F-G and Jiang X 2012 Flexoelectric strain gradient detection using $Ba_{0.64}Sr_{0.36}TiO_3$ for sensing *Appl. Phys. Lett.* **101** 252903–4
[24] Tagantsev A 1986 Piezoelectricity and flexoelectricity in crystalline dielectrics *Physi. Rev.* B **34** 5883
[25] Ma W 2008 A study of flexoelectric coupling associated internal electric field and stress in thin film ferroelectrics *Physica Status Solidi b* **245** 761–8
[26] Shu L, Wei X, Jin L, Li Y, Wang H and Yao X 2013 Enhanced direct flexoelectricity in paraelectric phase of Ba $(Ti_{0.87}Sn_{0.13})$ O_3 ceramics *Appl. Phys. Lett.* **102** 152904
[27] Yu J-C and Lan C-B 2001 System modeling of microaccelerometer using piezoelectric thin films *Sens. Actuators* A **88** 178–86
[28] Kwon S R 2014 Flexoelectricity of barium strontium titanate and its applications *Dissertation* North Carolina State University (http://www.lib.ncsu.edu/resolver/1840.16/10009)
[29] Lahiry S and Mansingh A 2008 Dielectric properties of sol-gel derived barium strontium titanate thin films *Thin Solid Films* **516** 1656–62
[30] Paek S-H, Won J, Lee K-S, Choi J-S and Park C-S 1996 Electrical and microstructural degradation with decreasing thickness of (Ba, Sr) TiO_3 thin films deposited by RF magnetron sputtering *Japan. J. Appl. Phys* **35** 5757
[31] Jiang X, Huang W and Zhang S 2013 Flexoelectric nano-generator: materials, structures and devices *Nano Energy* **2** 1079–92
[32] Lee W S and Lee S S 2008 Piezoelectric microphone built on circular diaphragm *Sensors Actuators* A **144** 367–73
[33] Narvaez J and Catalan G 2014 Origin of the enhanced flexoelectricity of relaxor ferroelectrics *Appl. Phys. Lett.* **104** 162903
[34] Rogalski A 2003 Infrared detectors: status and trends *Prog. Quantum Electron.* **27** 59–210
[35] Littrell R J 2010 High performance piezoelectric MEMS microphones *Dissertation* The University of Michigan (http://hdl.handle.net/2027.42/75833)
[36] Horowitz S B, Sheplak M, Cattafesta L N III and Nishida T 2006 A MEMS acoustic energy harvester *J. Micromech. Microeng.* **16** S174
[37] Martin D T, Liu J, Kadirvel K, Fox R M, Sheplak M and Nishida T 2007 A micromachined dual-backplate capacitive microphone for aeroacoustic measurements *J. Microelectromech. Syst.* **16** 1289–302
[38] Scheeper P R, Nordstrand B, Gullv J, Liu B, Clausen T, Midjord L and Storgaard-Larsen T 2003 A new measurement microphone based on MEMS technology *J. Microelectromech. Syst.* **12** 880–91
[39] Baumgartel L, Vafanejad A, Chen S-J and Kim E S 2013 Resonance-enhanced piezoelectric microphone array for broadband or prefiltered acoustic sensing *J. Microelectromech. Syst.* **22** 107–14